Deep-Space Optical Reception Antenna (DSORA): Aperture Versus Quality

J. V. Sandusky,[1] D. J. Hoppe,[2] and M. J. Britcliffe[2]

We report the relative diameter at which an optical antenna (telescope) having finite surface quality theoretically gathers the same amount of signal into the detector's field of view as a smaller antenna having a flawless surface. This relationship addresses a large range of errors from surface microroughness to surface figure error and panel misalignment, establishing a versatile guide for future trading of quality against aperture size in the specification of the primary mirror of the planned Deep Space Optical Reception Antenna (DSORA). We also report the ratio of background due to direct sunlight scattered from the primary mirror into the detector's field of view to background due to diffuse sky brightness, as a function of surface quality. This relationship determines a system-level trade space involving minimum operational Sun–Earth–probe (SEP) angle and surface quality. Limitations of the surface-roughness model employed are discussed.

I. Introduction

NASA's deep-space telecommunications road map [1] describes NASA's strategy for meeting the projected communication needs of future deep-space missions and their ever-increasing bandwidth requirements. While the addition of 32-GHz (Ka-band) downlink capability to the Deep Space Network (DSN) may suffice for the near future, the long-term plan calls for a move to optical links [2]. The key component in the ground segment of this planned optical communication link is the Deep Space Optical Reception Antenna (DSORA), a 10-meter-class optical antenna for collection of downlinked photons [3].

Unlike astronomical telescopes, the DSORA need not form an image but rather merely concentrate the incoming photons onto a detector. Without a requirement for imaging, the DSORA cost is expected to be much lower than the cost of an astronomical-quality telescope of the same aperture, such as the Keck telescopes. Also unlike most astronomical telescopes, the DSORA must operate not only at night but in daytime at close solar angles—its ability to track spacecraft near the Sun determines critical blackout periods for a given mission. This minimum angle, aside from possible thermo-mechanical design challenges arising from the sheer solar flux, will be determined by the tolerable amount of direct sunlight scattered into the detector by imperfections in the primary mirror.

This article proceeds by first describing the surface-error model and establishing the resulting optical point-spread function (PSF). Using the PSF, we then determine the fraction of the incident signal energy

[1] Communications Systems and Research Section.

[2] Communications Ground Systems Section.

The research described in this publication was carried out by the Jet Propulsion Laboratory, California Institute of Technology, under a contract with the National Aeronautics and Space Administration.

within the detector's field of view (FOV), P_E. This quantity is then expressed as the relative diameter, D/D_0, at which a mirror of diameter D having finite surface quality would gather the same amount of signal into the FOV as a smaller mirror of diameter D_0 having perfect surface quality. Next, we use the PSF to determine the surface quality at which scattering of direct sunlight from the primary mirror into the FOV becomes the dominant background source. We conclude with a summary of study results and an outline of future work.

Although we expect particulate contamination of the primary mirror to be a very substantial contributor to background level at narrow SEP angles, we restrict our analysis to the surface quality of the primary mirror and leave cleanliness effects as a matter for future work. Similarly, diffraction from the perimeter of the secondary mirror and its supporting structure are not considered.

II. Surface Quality

A. Random Surface Model

We take the antenna surface (primary mirror) to be normally distributed with surface error δz having zero mean and standard deviation σ as described in [4] and employed by Ruze in connection with radio frequency reflector antennas [5]. The surface autocorrelation function, $\beta(\delta x)$, is also taken to be normally distributed with standard deviation τ:

$$\beta\left(\delta x\right) = \left\langle \delta z\left(x\right) \delta z\left(x+\delta x\right)\right\rangle = \sigma^2 e^{-\left(\delta x/\tau\right)^2} \tag{1}$$

The standard deviation τ is referred to as the correlation length, giving the point where the autocorrelation function has dropped to a value of $1/e$ with respect its peak value, $\beta(0)$. In an approximate sense, surface errors within a distance τ may be considered to be correlated with each other, those further away to be roughly independent.

B. Point-Spread Function

Computation of the PSF for scattering by a random surface is discussed in many texts. In this brief discussion, the notation of Roggemann [6] is followed.

The point-spread function $S(\rho)$ at radius ρ from the optical axis is the Bessel transform

$$S\left(\rho\right) = 2\pi \int_0^\infty H\left(k\right) J_0\left(2\pi k\rho\right) k dk \tag{2}$$

of the optical transfer function

$$H\left(k\right) = \frac{\Gamma\left(\lambda f k\right)}{\Gamma\left(0\right)} \tag{3}$$

Here

$$\Gamma\left(\delta x\right) = \left\langle e^{j\theta(x)} e^{-j\theta(x+\delta x)} \right\rangle = e^{-\left(4\pi\sigma/\lambda\right)^2 \left[1-e^{-\left(\delta x/\tau\right)^2}\right]} \tag{4}$$

is the correlation of the phase function of the scattered field. Here k is the wave number $(2\pi/\lambda)$ with units 1/distance, and f is the system focal length. Due to the assumed isotropic nature of the random surface errors, the PSF is circularly symmetric.

The PSF may be written in terms of the infinite series [4]

$$S(\rho) = e^{-(4\pi[\sigma/\lambda])^2} \left[S_{DL}(\rho) + \frac{\pi}{\left(f\frac{\lambda}{\tau}\right)^2} \sum_{m=1}^{\infty} \frac{\left(4\pi\frac{\sigma}{\lambda}\right)^{2m}}{m \times m!} e^{-(1/m)(\pi[\rho/f(\lambda/\tau)])^2} \right] \tag{5}$$

where the diffraction-limited PSF $S_{DL}(\rho)$ is

$$S_{DL}(\rho) = \frac{\pi}{2} \frac{1}{\left(f\frac{\lambda}{D}\right)^2} \left[\frac{J_1\left(\pi\frac{\rho}{f[\lambda/D]}\right)}{\pi\frac{\rho}{f[\lambda/D]}} \right]^2 \tag{6}$$

The PSF $S(\rho)$ corresponds exactly to the far-field radiation pattern for a distorted reflector antenna computed by Ruze [5], appropriately transformed from the far-field to the focal plane.

In the following two subsections, we develop expressions for the signal energy and stray light on a detector in the focal plane.

C. Encircled Energy

The fraction of the incident signal focused onto the detector, P_E, is determined by integrating the PSF over the area of the detector:

$$P_E = 2\pi \int_0^{r_{det}} S(\rho)\, \rho d\rho \tag{7}$$

where r_{det} is the radius of the detector. Performing the integration results in

$$P_E(FOV) =$$

$$1 - e^{-(4\pi[\sigma/\lambda])^2} \left\{ J_0^2\left(\pi \frac{\frac{FOV}{2}}{\frac{\lambda}{D}}\right) + J_1^2\left(\pi \frac{\frac{FOV}{2}}{\frac{\lambda}{D}}\right) + \sum_{m=1}^{\infty} \frac{\left(4\pi\frac{\sigma}{\lambda}\right)^{2m}}{m!} e^{-(1/m)(\pi[FOV/2]/[\lambda/\tau])^2} \right\} \tag{8}$$

where

$$FOV = \frac{2r_{det}}{f} \tag{9}$$

is the full field of view of the detector. In all cases of interest here, the field of view will be large compared with the diffraction limit of the aperture, ($FOV \gg \lambda/D$), and Eq. (8) may be simplified to

$$P_E(FOV) = 1 - e^{-(4\pi[\sigma/\lambda])^2} \sum_{m=1}^{\infty} \frac{\left(4\pi\frac{\sigma}{\lambda}\right)^{2m}}{m!} e^{-(1/m)(\pi[(FOV/2)/(\lambda/\tau)])^2}, \quad \left[FOV \gg \frac{\lambda}{D}\right] \tag{10}$$

In the limit that the rms surface roughness goes to zero, ($\sigma \to 0$), the encircled energy approaches unity, as expected.

It is useful to consider the ratio

$$\frac{D}{D_0} = \frac{1}{\sqrt{P_E}} \tag{11}$$

of the diameter D of a mirror having finite surface quality to the diameter D_0 of a smaller yet flawless mirror that would concentrate an equal amount of signal onto the detector, as plotted in Fig. 1. The series [Eq. (10)] can be slowly convergent for some sets of parameters and was approximately summed as described in the Appendix.

Figure 1 shows that a factor-of-two increase in receiver diameter permits several waves (several λ) of error if the correlation length τ is longer than $\sim 10\lambda/FOV$ (or, equivalently, if the detector FOV is larger than about 10 times the correlation-length limit, λ/τ). Also, if the surface is relatively smooth ($\sigma < \lambda/10$), the increase in diameter becomes independent of correlation length for $\tau < 0.3\lambda/FOV$. This means that the efficiency of the receiver is independent of the scale of microfeatures as long as they are relatively smooth. For instance, if the detector field of view were 100 μrad and the wavelength 1 μm, features shorter than 3 mm having less than 100 nm of rms roughness would require a receiver only twice as large as a receiver having a perfectly smooth surface.

Figure 2 provides detail to Fig. 1 for relative diameters between one and two, and utilizes a linear scale. It shows that if the rms surface roughness, σ, were 5 percent of the signal wavelength, λ, and the FOV were 30 percent of the correlation-length limit, λ/τ, the primary mirror would need to be 18 percent larger than if it had perfect surface quality. The mirror would need to be twice as large if the rms surface roughness increased to 10 percent of the signal wavelength. On the other hand, if the detector's FOV were equal to the correlation-length limit, the diameter need be only 10 percent larger; as long as the detector's FOV remains close to the correlation-length limit, the mirror need not be substantially larger even for rough surfaces. Figure 3 repeats Fig. 2 for the specific case of $FOV = 100$ μrad and $\lambda = 1$ μm, providing the correlation length and rms surface roughness in meters.

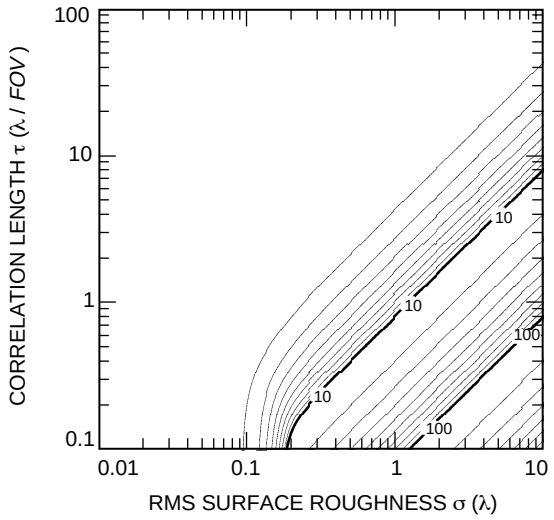

Fig. 1. Telescope diameter *D* for a mirror having finite surface quality normalized by the diameter D_0 of a smaller yet flawless mirror that would concentrate an equal amount of signal onto the detector. The correlation length τ is normalized with respect to (λ / *FOV*) and σ with respect to λ.

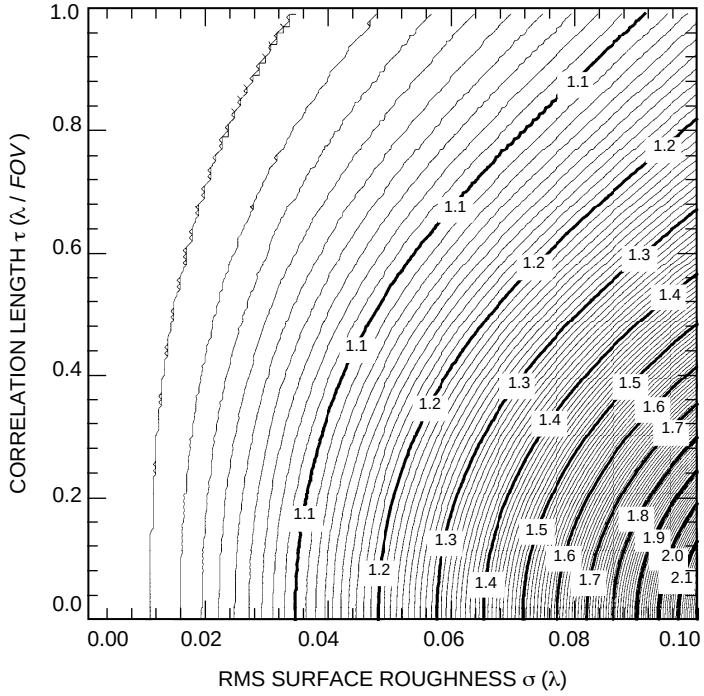

Fig. 2. An expanded version of Fig. 1 presented on a linear scale. The correlation length τ is normalized with respect to (λ / *FOV*) and σ with respect to λ.

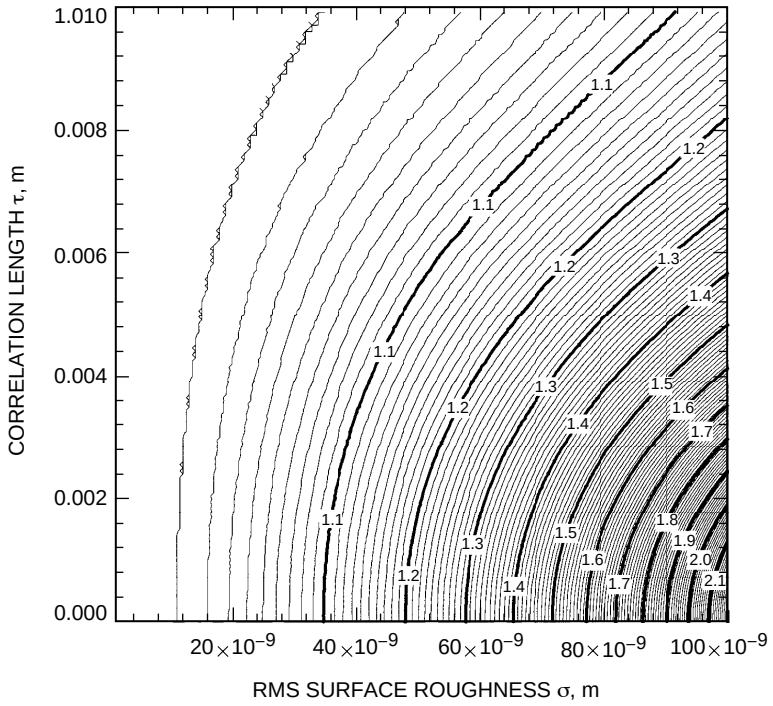

Fig. 3. A repeat of Fig. 2 for the specific case of *FOV* = 100 μrad and λ = 1 μm, providing the correlation length and rms surface roughness in meters.

D. Stray-Light Rejection

During daytime operation at close solar angles, there are two dominant sources of background light: (1) diffuse sky brightness within the detector's field of view and (2) direct sunlight scattering from the surface of the primary mirror into the detector's field of view. If the diffuse sky brightness is approximated as uniform over the sky dome, the amount of diffuse sky brightness encircled by the detector is approximately independent of surface quality: while surface flaws reduce background from diffuse sky brightness within the detector's geometrical field of view, they increase background from diffuse sky brightness outside the detector's geometrical field of view by the same amount. Equivalently, the surface flaws change the shape of the detector's radiation pattern but not its integrated value. Since the diffuse sky brightness, P_{DIF}, depends in general on the portion of sky observed, the time of day, the season, the wavelength, the polarization, the atmospheric constituents, and the weather, we take a nominal value of 100 mW per square meter per steradian per nanometer of spectral filter bandwidth [7]. Using this constant, the diffuse sky brightness encircled by the detector is

$$P_{DIF} = \frac{100\ \text{mW}}{\text{m}^2}\ \frac{1}{\text{nm}}\ \frac{1}{\text{sr}}\pi\left(\frac{D}{2}\right)^2 \times \Delta\lambda \times \pi\left(\frac{FOV}{2}\right)^2 \tag{12}$$

where D is the aperture diameter and $\Delta\lambda$ is the spectral filter bandwidth.

The second source of background light, on the other hand, depends strongly on the surface roughness and correlation length. Consider the focal plane depicted in Fig. 4, where the detector and the Sun are separated by an angle, *SEP*. For ease of evaluation, we have arranged the geometry so that the telescope is pointed directly at the Sun with the detector being off-axis, and we take the Sun to be a point source. The extended nature of the Sun can be reintroduced in a conservative fashion by measuring the SEP angle from its edge. The direct solar energy scattered by the primary mirror into the detector's field of view is approximately the fraction of the incident solar energy encircled in the sector of the ring containing the detector:

$$P_{\text{SUN}} \approx \frac{1\ \text{W}}{\text{m}^2}\ \frac{1}{\text{nm}}\pi\left(\frac{D}{2}\right)^2 \times \Delta\lambda\frac{FOV/SEP}{2\pi}\left[P_E\left(SEP + \frac{FOV}{2}\right) - P_E\left(SEP - \frac{FOV}{2}\right)\right] \tag{13}$$

where we have approximated the solar constant as 1 W per square meter per nanometer of spectral bandwidth. If $FOV/2 \ll SEP$, we can approximate P_{SUN} in terms of the derivative of P_E:

$$P_{\text{SUN}} \approx \frac{1\ \text{W}}{\text{m}^2}\ \frac{1}{\text{nm}}\pi\left(\frac{D}{2}\right)^2 \times \Delta\lambda\frac{FOV^2/SEP}{2\pi}\ \frac{d}{dSEP}\ P_E\left(SEP\right), \quad \left[\frac{FOV}{2} \ll SEP\right] \tag{14}$$

Performing the derivative analytically results in the series

$$P_{\text{SUN}} = \frac{1\ \text{W}}{\text{m}^2}\ \frac{1}{\text{nm}}\pi\left(\frac{D}{2}\right)^2 \times \Delta\lambda\frac{\pi}{4}\left(\frac{FOV/2}{\lambda/\tau}\right)^2 e^{-(4\pi[\sigma/\lambda])^2}\sum_{m=1}^{\infty}\frac{\left(4\pi\frac{\sigma}{\lambda}\right)^{2m}}{m!}\ \frac{1}{m}\ e^{-(1/m)(\pi[(SEP/2)/(\lambda/\tau)])^2} \tag{15}$$

which when normalized by P_{DIF} and SEP^2 produces the highly general result

$$SEP^2\frac{P_{\text{SUN}}}{P_{DIF}} = 10\frac{\pi}{4}\left(\frac{SEP/2}{\lambda/\tau}\right)^2 e^{-(4\pi[\sigma/\lambda])^2}\sum_{m=1}^{\infty}\frac{\left(4\pi\frac{\sigma}{\lambda}\right)^{2m}}{m!}\ \frac{1}{m}e^{-(1/m)(\pi[(SEP/2)/(\lambda/\tau)])^2} \tag{16}$$

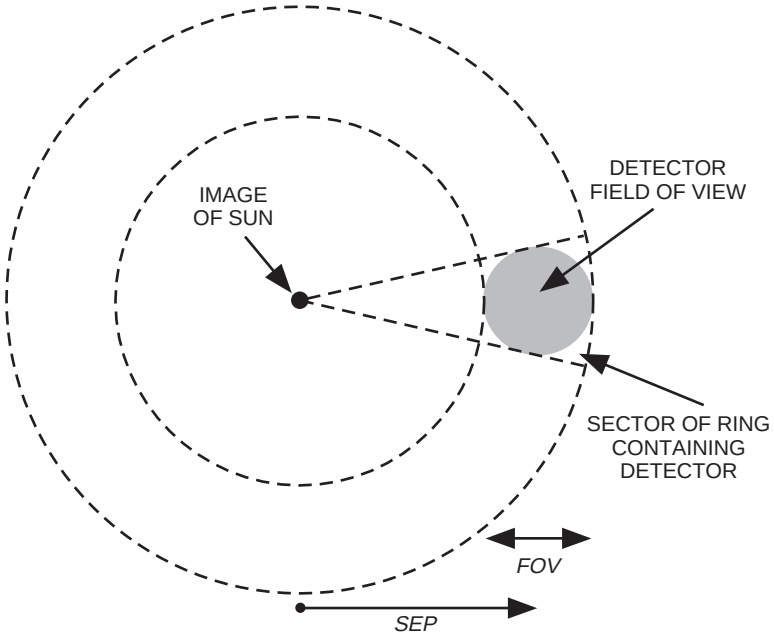

Fig. 4. The focal-plane configuration used for stray-light computation.

Equation (16) shows that, under these approximations, the ratio of the background from scattered direct sunlight to the background from diffuse sky brightness is independent of the filter bandwidth, the aperture diameter, and the detector field of view. Once again this sum may be slowly convergent and is summed using the approximate technique presented in the Appendix.

A general contour plot of Eq. (16) is presented as Fig. 5. Note that for relatively smooth surfaces ($\sigma < \lambda/10$) and long correlation lengths ($\tau > \lambda/SEP$) the gradient is extremely large, with order-of-magnitude changes in the ratio $SEP^2 \times P_{\rm SUN}/P_{DIF}$ occurring over only fractional changes in rms roughness. For rough surfaces ($\sigma > \lambda$), on the other hand, the gradient is much smaller and roughly independent of correlation length. Also, note that there exists a worst-case contour giving the largest possible contribution from scattered direct sunlight. The physical explanation is that, for relatively smooth surfaces, scattering from surface irregularities remains near-specular and tightly concentrated. Increases in the rms surface roughness or decreases in the correlation length cause the mean scattering angle to increase, bringing the scattered light closer to the detector. As the beam is tightly concentrated, small changes in the mean scattering angle result in large changes in the fraction of scattered light incident on the detector. The worst-case occurs for the line $4\pi\sigma/\tau \sim SEP$; the ratio $4\pi\sigma/\tau$ acts physically as the mean angle of reflection from surface flaws. The reduced gradient for higher rms roughness or smaller correlation length indicates that the scattered beam is diffuse and, therefore, the fraction of the scattered light reaching the detector is less sensitive to the mean angle of reflection from surface flaws.

A contour plot of the ratio $P_{\rm SUN}/P_{DIF}$ for the specific case of $\lambda = 1$ μm and $SEP = 1$ deg is presented as Fig. 6. An SEP angle of 1 deg is chosen since, for current DSN operation at X-band, this SEP angle gives an approximate noise increase of 3 dB [8]. The curve having unit value (10^0) defines the relationship between correlation length and rms surface roughness that will produce equal amounts of background from diffuse sky brightness and scattering of direct sunlight from the primary mirror. Curves to the right of the unit curve are dominated by scattering of direct sunlight, those to the left by the diffuse sky brightness. Surface features having correlation lengths of $\sim$0.2 mm permit 100 nm of rms surface roughness with longer correlation lengths permitting linearly increasing surface roughness. Surface features having correlation lengths shorter than $\sim$100 μm require surface roughness less than 10 nm, although features with very short correlation lengths of $\sim$10 μm will permit surface roughness larger than 10 nm.

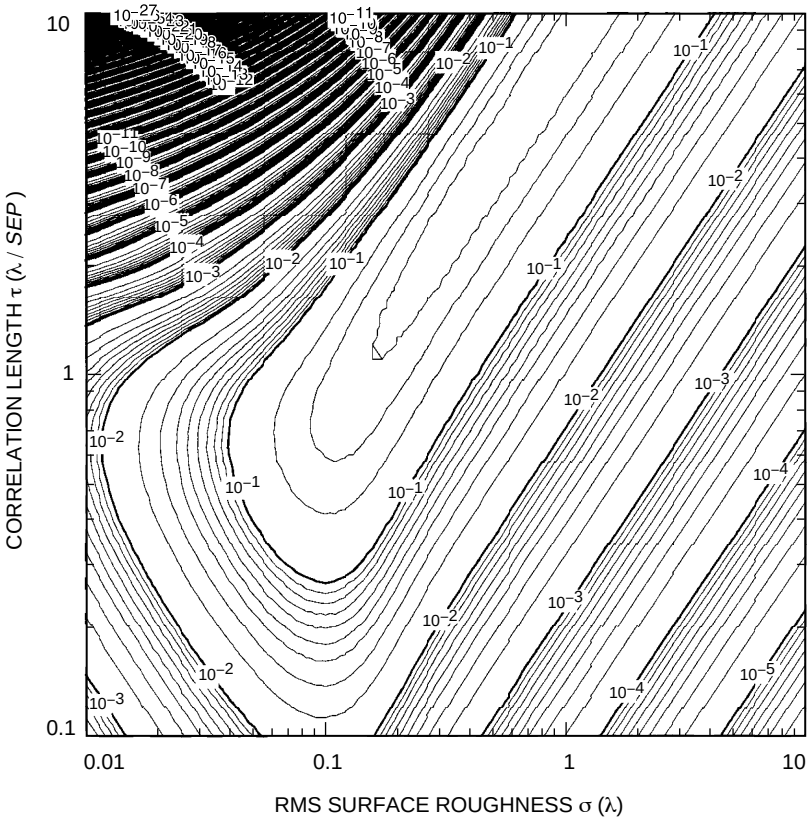

Fig. 5. Scattered direct sunlight normalized by the diffuse sky brightness / *SEP*^{2} versus correlation length and rms surface roughness. The correlation length τ is normalized with respect to (λ / *SEP*) and σ with respect to λ.

E. Relationship to the BRDF

Measured scattering from optical surfaces is usually described in terms of the bidirectional reflectance distribution function (BRDF) [9], which gives the fraction of an incident beam scattered per steradian into a particular direction. The BRDF is convenient for both measurement and calculation. Although Beckman did not relate his Gaussian-random model to the BRDF, Stover [10] produced the explicit relationship for the rough-surface limit. Although in general the relationship between the measured BRDF and the surface statistics has not been solved, for smooth surfaces the BRDF is closely related to the PSF, and the autocorrelation function can be calculated from the Fourier transform of the BRDF within the spatial frequency limits of the measurement.

F. Limitations of the Gaussian Model

The Gaussian-random model of surface autocorrelation and height distribution is employed chiefly for its simplicity and breadth and for easy comparison with previous DSORA surface-error studies [3]. Real surfaces do not in general closely conform to the Gaussian model; most measured materials [9] have exponential autocorrelation functions rather than Gaussian. Also, real surfaces, especially those that have been machined, tend to have significant periodic surface features that are not modeled by the Gaussian function. Finally, the validity of the Gaussian-random model is restricted to the Kirchoff regime ($\tau \gg \lambda$). Despite these limitations, the Gaussian model is useful as a guide for estimating the effect of surface microroughness and figure errors on encircled energy and stray light.

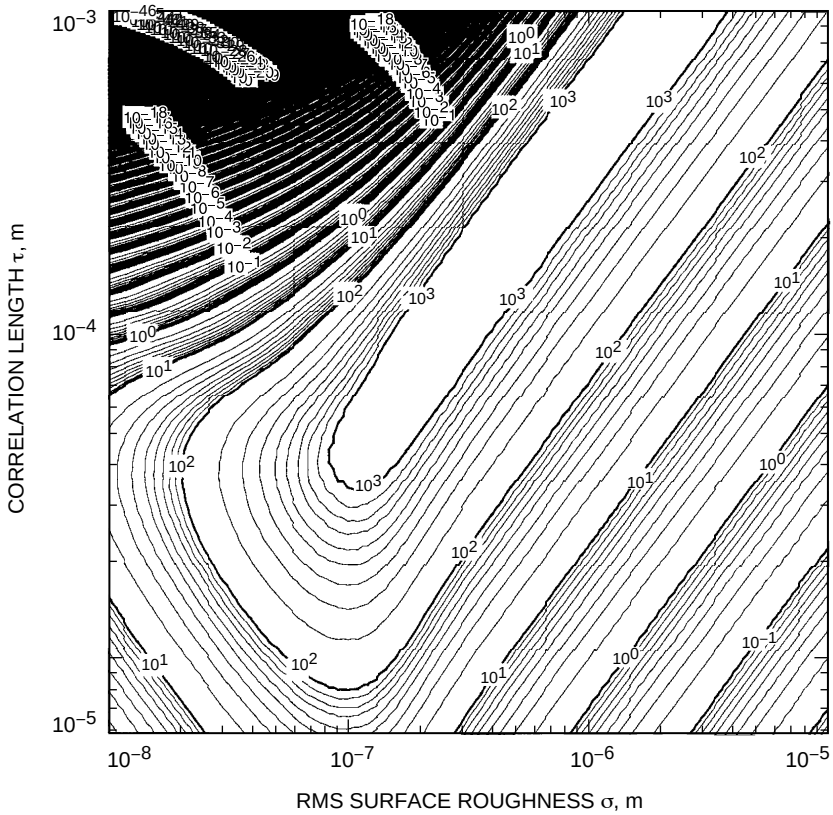

Fig. 6. The ratio P_{SUN} / P_{DIF} for the specific case of $\lambda = 1$ μm and *SEP* = 1 deg.

III. Conclusions

Because of scattering of direct sunlight onto the detector, the surface microroughness specification for the DSORA will be driven by the minimum Sun–Earth–probe angle at which operation is required. The dependence of DSORA throughput on surface figure error and microroughness has been determined, within the limitations of the Gaussian random model, and stated in terms of the diameter of an equivalent perfect surface. Preliminary investigations indicate that potentially low-cost diamond-turned mirrors appear to satisfy a 1-deg SEP-angle requirement while not requiring a substantially larger aperture.

IV. Future Work

Armed with the results of this study, future work should focus on identifying cost-effective measures for producing main-reflector panels for the DSORA that will provide acceptable signal collection and stray-light rejection. Maintenance of the surface figure using panel actuators must be investigated as well, always keeping in mind the much-reduced DSORA requirements relative to imaging instruments. With appropriate cost information and the performance results of this study, an appropriate system-level trade-off of cost versus overall performance, signal collection, and stray light can be made. In addition, the issue of surface cleanliness must be addressed since it is likely to be a significant factor in the stray-light rejection capability of the DSORA. The effects of periodic tool marks must be investigated as well, although this is expected to be a relatively straightforward task.

References

[1] C. D. Edwards, Jr., C. T. Stelzried, L. J. Deutsch, and L. Swanson, "NASA's Deep-Space Telecommunications Road Map," *The Telecommunications and Mission Operations Progress Report 42-136, October–December 1998*, Jet Propulsion Laboratory, Pasadena, California, pp. 1–20, February 15, 1999. http://tmo.jpl.nasa.gov/tmo/progress_report/42-136/136B.PDF

[2] K. Shaik, D. Wonica, and M. Wilhelm, "Optical Subnet Concepts for the Deep Space Network," *The Telecommunications and Data Acquisition Progress Report 42-115, July–September 1993*, Jet Propulsion Laboratory, Pasadena, California, pp. 1–29, November 15, 1993. http://tmo.jpl.nasa.gov/tmo/progress_report/42-115/115m.pdf

[3] K. Shaik, "Progress on Ten-Meter Optical Receiver Telescope," *Free Space Laser Communication Technologies IV*, SPIE vol. 1635, pp. 109–117, 1992.

[4] P. Beckmann and A. Spizzichino, *The Scattering of Electromagnetic Waves from Rough Surfaces*, Norwood, Massachusetts: Artech House, 1987.

[5] J. Ruze, "Antenna Tolerance Theory—A Review," *Proc. IEEE*, vol. 54, pp. 633–640, April 1966.

[6] M. C. Roggemann and B. Welsh, *Imaging Through Turbulence*, New York: CRC Press, 1996.

[7] Y. Liu and K. Voss, "Polarized Radiance Distribution Measurement of Skylight. II. Experiment and Data," *Applied Optics*, vol. 36, no. 33, pp. 8753–8764, 1997.

[8] S. D. Slobin, *DSN/Flight Project Interface Design Handbook*, JPL Document 810-5, Rev. D, vol. I, "DSN Telecommunications Interfaces 70 Meter Antenna Subnet," TCI-10, Rev. G, Jet Propulsion Laboratory, Pasadena, California, January 15, 1997.

[9] J. M. Bennett and L. Mattsson, *Introduction to Surface Roughness and Scattering*, 2nd edition, Washington, D.C.: Optical Society of America, 1999.

[10] J. C. Stover, *Optical Scattering Measurement and Analysis*, 2nd edition, Bellingham, Washington: SPIE—The International Society for Optical Engineering, p. 192–193, 1995.

Appendix
Numerical Summation of P_E

The exponential term in the series

$$\sum_{m=1}^{\infty} \frac{\left(4\pi\frac{\sigma}{\lambda}\right)^{2m}}{m!} e^{-(1/m)(\pi[FOV/2]/[\lambda/\tau])^2} \tag{A-1}$$

increases in magnitude with m and, for $4\pi\sigma > \lambda$, the power term likewise increases. Though the factorial term assures convergence, the series converges only slowly. For numerical computation, it is necessary to truncate the series and to have a bound on the error introduced by truncation. To estimate a useful truncation point, we bring all of the terms into the exponent and invoke Sterling's approximation

$$\ln(m!) \approx \frac{1}{2}\ln(2\pi) + m\ \ln(m) + \frac{1}{2}\ln(m) - m, \quad [m_{max} \gg 1] \tag{A-2}$$

Taking the derivative with respect to m shows that the term m_{max} satisfying

$$2\ln\left(4\pi\frac{\sigma}{\lambda}\right) - \ln(m_{max}) - \frac{1}{2m_{max}} + \frac{1}{m_{max}^2}\left(\pi\frac{FOV/2}{\lambda/\tau}\right)^2 = 0, \quad [m_{max} \gg 1] \tag{A-3}$$

makes the largest contribution to the summation. The transcendental nature of this equation makes it difficult to solve analytically. However, the left-hand side of Eq. (A-3) is positive for small m_{max} and negative if both

$$m_{max} > \left(4\pi\frac{\sigma}{\lambda}\right)^2 \tag{A-4a}$$

and

$$m_{max} > 2\pi\,\frac{FOV/2}{\lambda/\tau} \tag{A-4b}$$

A somewhat arbitrary truncation point can then be established as $3m_{max}$, where

$$m_{max} \sim \left(4\pi\frac{\sigma}{\lambda}\right)^2 + 2\pi\,\frac{FOV/2}{\lambda/\tau} \tag{A-5}$$

Equation (A-1) is then approximated:

$$\sum_{m=1}^{\infty} \frac{\left(4\pi\frac{\sigma}{\lambda}\right)^{2m}}{m!} e^{-(1/m)(\pi[FOV/2]/[\lambda/\tau])^2} \approx \sum_{m=1}^{3m_{max}} \frac{\left(4\pi\frac{\sigma}{\lambda}\right)^{2m}}{m!} e^{-(1/m)(\pi[FOV/2]/[\lambda/\tau])^2} \tag{A-6}$$

An upper bound on the error introduced by truncating the summation is provided by integrating over the remaining terms. For the figures presented in this article, the integrated remaining terms had magnitude $<10^{-20}$.